Supplementary information for: "Unveiling the complex organization of recurrent patterns in spiking dynamical systems"

March 26, 2014

Andrés Aragoneses[1], Sandro Perrone[1], Taciano Sorrentino[1,2], M. C. Torrent[1], and Cristina Masoller[1]

[1] Departament de Física i Enginyeria Nuclear, Universitat Politècnica de Catalunya, Colom 11, Terrassa, 08222 Barcelona, Spain
[2] Departamento de Ciências Exatas e Naturais, Universidade Federal Rural do Semi-Árido, 59625-900 Mossoró, RN, Brazil

Detection of the spike times

Figure 1 displays, as examples, typical intensity time traces at low and high pump current (26.5 mA and 27.3 mA for the experimental data and $\mu = 0.98$ and 1.01 for the numerical data). For both, the following method was used to detect the times when the spikes occur. First, each time series was normalized to have zero mean value and standard deviation equal to one. Next, the spike times were determined by using a simple thresholding method: when the intensity decreases below a certain value, a spike is recorded. Then, it was required that the intensity grows above zero before another spike can occur. This avoids detecting spurious spikes, specially during the intensity recovery (the dropout is sharp but the recovery is gradual and noisy). Alternatively, one could use a "refractory time" after each dropout, during which the intensity is recovering and no spikes are detected.

To verify the method of spike detection we compare the mean inter-spike interval, $\langle \Delta T \rangle$, and the normalized standard deviation, $\sigma / \langle \Delta T \rangle$, for experimental and simulated data. Figure 2 displays $\langle \Delta T \rangle$ and $\sigma / \langle \Delta T \rangle$ vs. the pump current (experimental data), and vs. the parameter μ (numerical data), calculated using a

spike detection threshold equal to -2. A good qualitative agreement experiments-simulations can be observed, and the variation of $\langle \Delta T \rangle$ and $\sigma / \langle \Delta T \rangle$ with the pump current is also in good agreement with previous observations [1, 2].

To further verify the method of spike time detection, we calculated the histograms of ΔT values. Figure 3 displays the histograms corresponding to the time series shown in Fig. 1, again computed with a threshold of -2. We observe a good qualitative agreement of the experimental and numerical histograms, which are also in good agreement with previous reports [3, 4]. We note that for low pump current, in the numerical histogram (Fig. 3b) there is a sharp peak at low ΔT values, that is not seen in the experimental histogram (Fig. 3a). The reason of this peak is the presence of intermittent bursts of regular spikes. This regular dynamics has been observed experimentally in the literature and has been referred to as *regular pulse packages* [5, 6]. Because the regular spikes are not as deep as the irregular ones (Fig. 4a), by choosing a deeper threshold (e.g., -2.5) they are not detected and the peak in the histogram of ΔT values is eliminated, as seen in Fig. 4b.

Influence of the detection threshold in the word probabilities

Next, we analyze the influence of the detection threshold in the probabilities of the ordinal patterns. Figure 5 shows the probabilities vs. the detection threshold, for the same pump currents as in Fig.1. It can be appreciated that, while the values of the probabilities vary with the threshold, the hierarchy and the clusters (021-102 and 120-201) are robust and occur in a wide range of threshold values. While for too low (or too deep) thresholds the probabilities vary significantly (as too many or too few spikes are detected), they are robust to threshold variations in a wide range of thresholds.

Most importantly, the variation of the probabilities with the threshold is qualitatively the same in the experimental and in the numerical data. The same hierarchy and clusters are seen. This is remarkable because the model used for the simulations is the simplest rate-equation model (assumes single-mode emission, neglects spatial and thermal effects, considers only optical noise, etc.) and the filter used to simulate the finite detection bandwidth is also a simple moving-average window.

While an optimal threshold could be defined for each pump current value (that is in the center of the “plateau” where the probabilities do not vary significantly with the threshold), for the sake of simplicity in our work we used a fixed threshold value, equal to -2, for detecting the spikes.

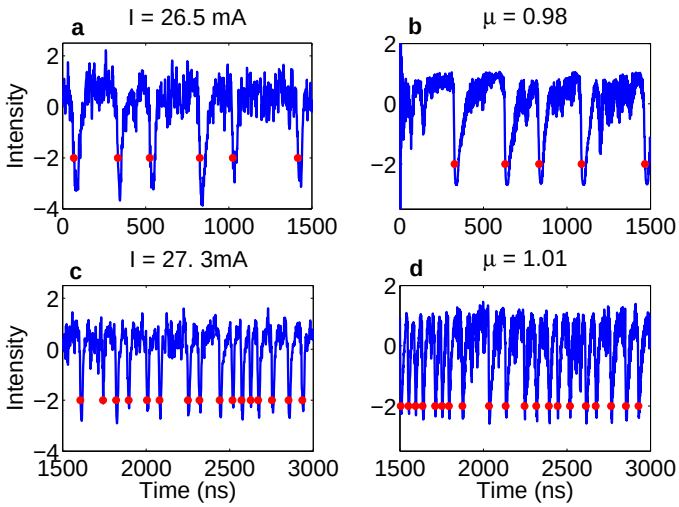

Figure 1: Typical time series of the laser intensity. Panels **a** and **c** display experimental data (the pump current is 26.5 mA and 27.3 mA respectively) and panels **b** and **d**, numerical data (the pump current parameter is $\mu = 0.98$ and 1.01 respectively). The dots indicate the times when a spike is detected using a threshold equal to -2. In the simulations $\eta = 20$ ns^{-1} and $\alpha = 4.5$, other parameters are as indicated in Methods.

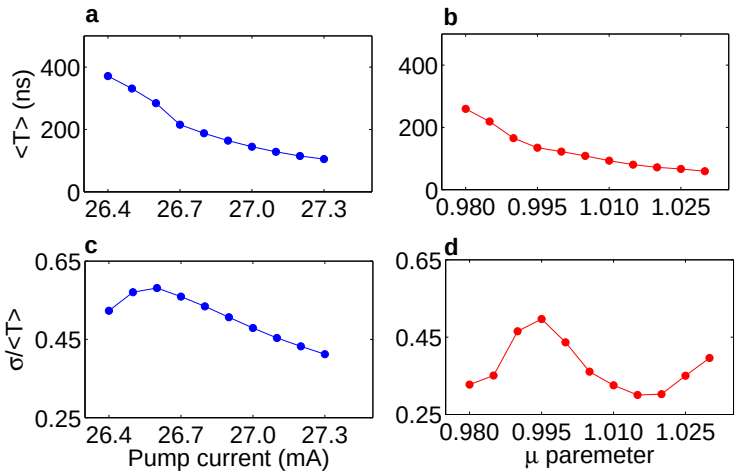

Figure 2: **a, b** Mean inter-spike interval and **c, d** normalized standard deviation versus the pump current, for experimental data **a, c** and for numerical data **b,d**. The threshold for detecting the spike times is -2 and the parameters of the simulation are as in Fig. 1.

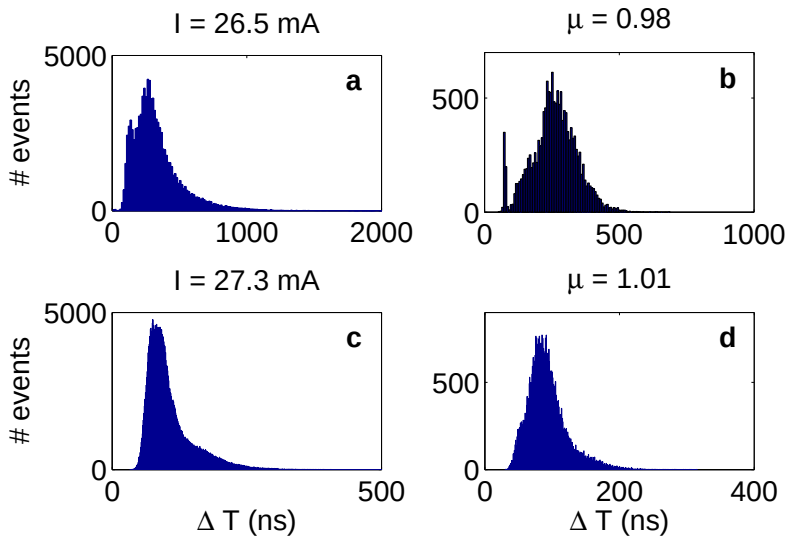

Figure 3: Histograms of the inter-spike intervals corresponding to the time series shown in Fig. 1.

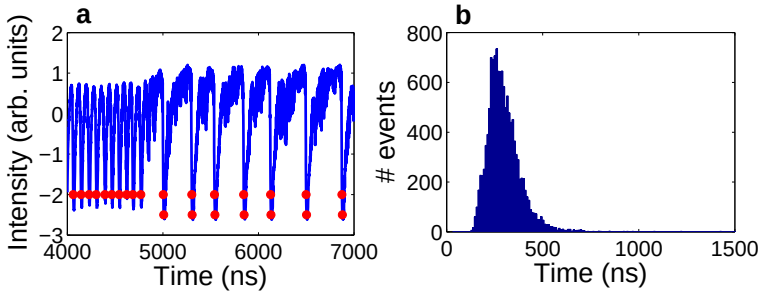

Figure 4: **a** Detail of the regular pulse packages in the simulated time-series for $\mu = 0.98$. The dots indicate two thresholds for detecting the spike times. Panel **b** displays the histogram of ΔT values computed by using the lower threshold (-2.5).

Calculation of the error bars of probability values and the null hypothesis region.

In order to determine if the word probabilities are consistent with a distribution of equally probable words (null hypothesis, N.H., of no correlations present in the spike sequence), we calculate the error bars of the probabilities as well as the probability region consistent with the N.H. They are calculated as in Ref. [7]: using a binomial test to compute the error bars, and using a confidence level of 95% for the N.H. region: $p \pm 3\sigma_p$, where $p = 1/D!$ and $\sigma_p = \sqrt{(p(1-p)/N)}$, with D being the length of the word and N the number of words in the sequence.

Figures 6a-c display the results for words of length $D = 2$, 3 and 4 respectively. One can clearly observe that the distribution of probability values is not consistent with the N.H., as several probabilities are outside the N.H. region (gray region in Fig. 6). For the sake of clarity, Fig. 6d displays the probabilities of words of length $D = 4$ computed from surrogate data (shuffled inter-spike intervals time series), and we can confirm that in this case the probabilities are all within the gray region.

Analysis of spike correlations

To further confirm the presence of correlations in the spike sequence, we compute the usual autocorrelation coefficient of the sequence of inter-spike intervals, $\{\Delta T_i\}$, as

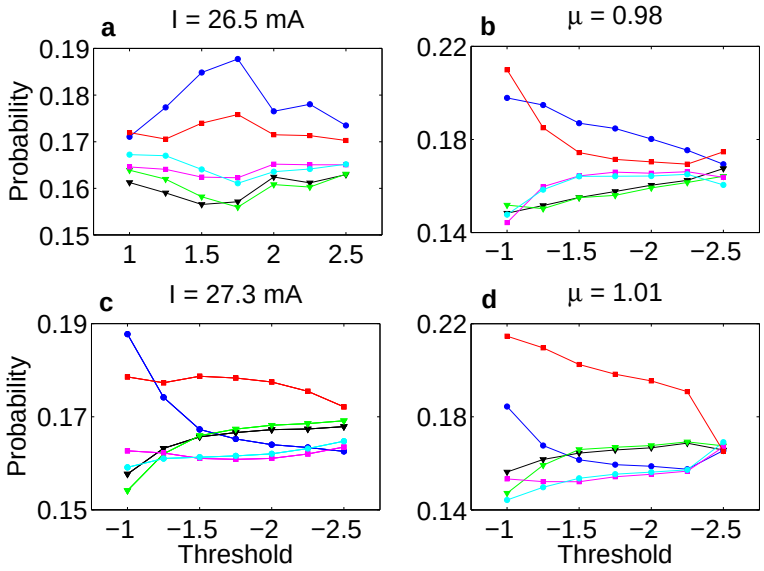

Figure 5: Probabilities of the words vs. the detection threshold is shown for different pump current values both, for the experimental **a, c** and the simulations **b, d** data.

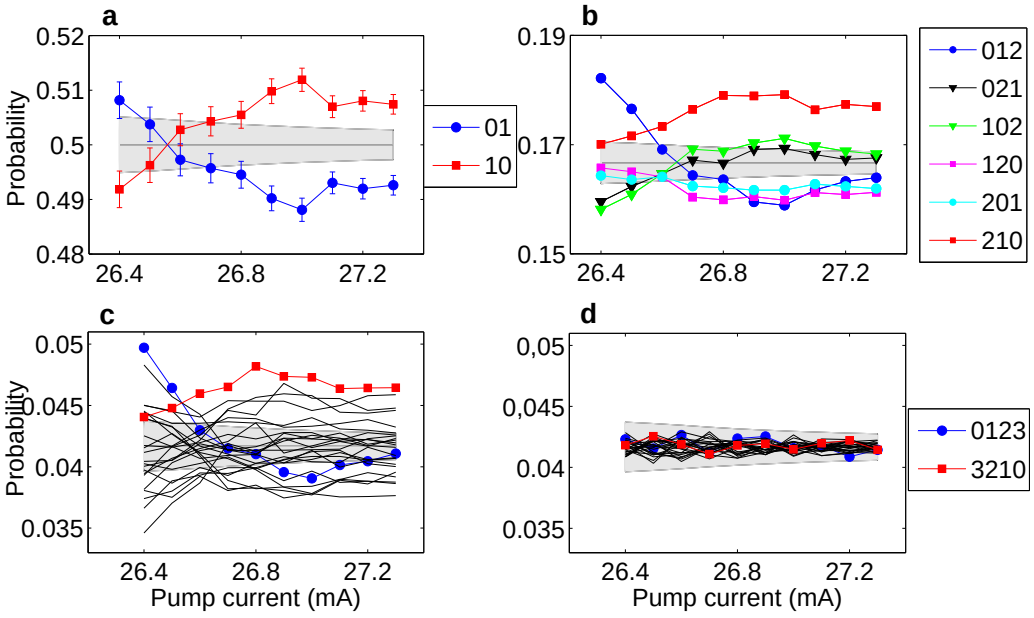

Figure 6: Probabilities of the words of length, **a** $D = 2$, **b** $D = 3$ and **c** $D = 4$ vs. the pump current, computed from the experimental data. The words '012' and '210' present the same crossover as words '01' and '10', and '0123' and '3210' (blue and red, respectively in panel **c**. Panel **d** displays the probabilities for $D = 4$ computed from the surrogated data (shuffled inter-spike intervals time series).

$$C_\tau = \frac{\langle (\Delta T_i - \langle \Delta T \rangle)\,(\Delta T_{i-\tau} - \langle \Delta T \rangle) \rangle}{\sigma^2} \tag{1}$$

The result is shown in Fig. 7, that displays C_1 and C_2 vs. the pump current for the experimental data. First-order correlations are clearly identified, which are stronger at low pump currents, while second-order correlations are significantly weaker.

From these results we can also confirm that the symbolic ordinal analysis indeed provides additional information with respect to the usual correlation analysis. In particular, we notice that C_1 is positive for all current values; however, in Fig. 6a we see that at high currents the word '10' is more probable (i.e., $\Delta T_i > \Delta T_{i+1}$ is more probable than $\Delta T_i < \Delta T_{i+1}$), and at low currents, it is the opposite situation (the word '01' is more probable, and thus, $\Delta T_i < \Delta T_{i+1}$ is more probable than $\Delta T_i > \Delta T_{i+1}$). This is apparently contradictory; however, one should keep in mind that the ordinal analysis takes into account the relative values of consecutive intervals, while the correlation coefficient, takes into account the magnitude of consecutive $\Delta T_i - < \Delta T >$ values. Moreover, Fig. 7 shows that C_2 is very small, suggesting negligible correlations; however the probabilities of the words of length $D = 3$ are clearly not consistent with the N.H.

Delay embedding analysis

A well-known method for reconstructing the attractor of a dynamical system is to compute a delay embedding of the inter-spike intervals [8]. To explore this method we consider several embedding dimensions (m=1, m=2, and m=3) and plot the three-dimensional reconstruction of the attractor for the experimental and for the simulated data (see Fig. 8). No well-defined attractor can be inferred by this technique, but rather an apparently random cloud of data points. This reinforces the relevance of the symbolic ordinal method used in this work, that it can unveil an underlying structure in the sequence of inter-dropout intervals, which can not be revelead by the reconstruction method. In the case of the circle map model (right column) a noisy but clear structure can be appreciated. Therefore, the suitability of the circle map to describe the LFFs dynamics of a semiconductor laser with feedback is limited to the serial correlations present in the sequence of dropouts, and the dimensionality of the dynamics or the statistical distribution of inter-spike interval values are not well described by this minimal model.

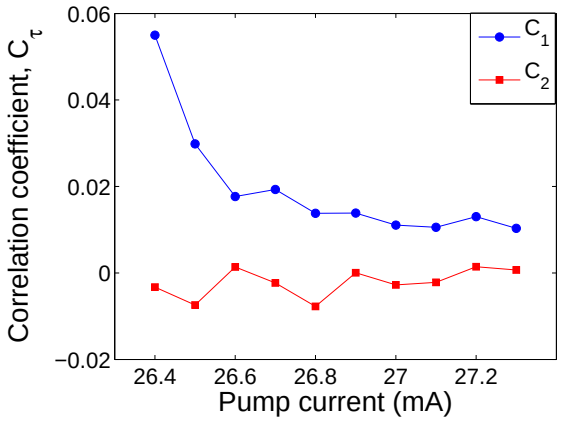

Figure 7: First and second order correlation coefficient of the inter-spike interval sequence, C_1 and C_2 [Eq. 1], computed from the experimental data, as a function of the laser pump current.

To analyze the length of the serial correlations present in the sequence of inter-dropout intervals, we construct the words using a delay m, i.e., the words are formed as (ΔT_i, T_{i+m}, ΔT_{i+2m}). The probabilities of the words defined in this way are presented in Fig. 9, for the experimental data (left column) and for the numerical data (right column). The probabities are outside the gray region (consistent with the null hypotesis) only for the lowest embedding dimension, revealing that the serial correlations only extend to a few inter-spike intervals.

Additional experimental measurements

In order to demonstrate the robustness of our observations, we performed several experiments employing different lasers and feedback conditions. Figures 10a and 10b display the probabilities computed with data analyzed in our previous work [7]. In that experiment we used a different laser (Hitachi Laser Diode HL 6724 MG), lasing at 675 nm, with a shorter external cavity (45 cm corresponding to 3 ns of time delay), and a feedback-induced threshold reduction was 7%). Two data sets were recorded at different temperatures (18 C in panel a, 20 C in panel b). One can observe that in both data sets, the hierarchy, clusters and crossover are the same as in Fig. 6b. For Fig. 10c the strength of the optical feedback is weaker, resulting in a threshold reduction of 4%. Also the two clusters and a crossover (such that the word 210 becomes the most probable one at high current) are seen

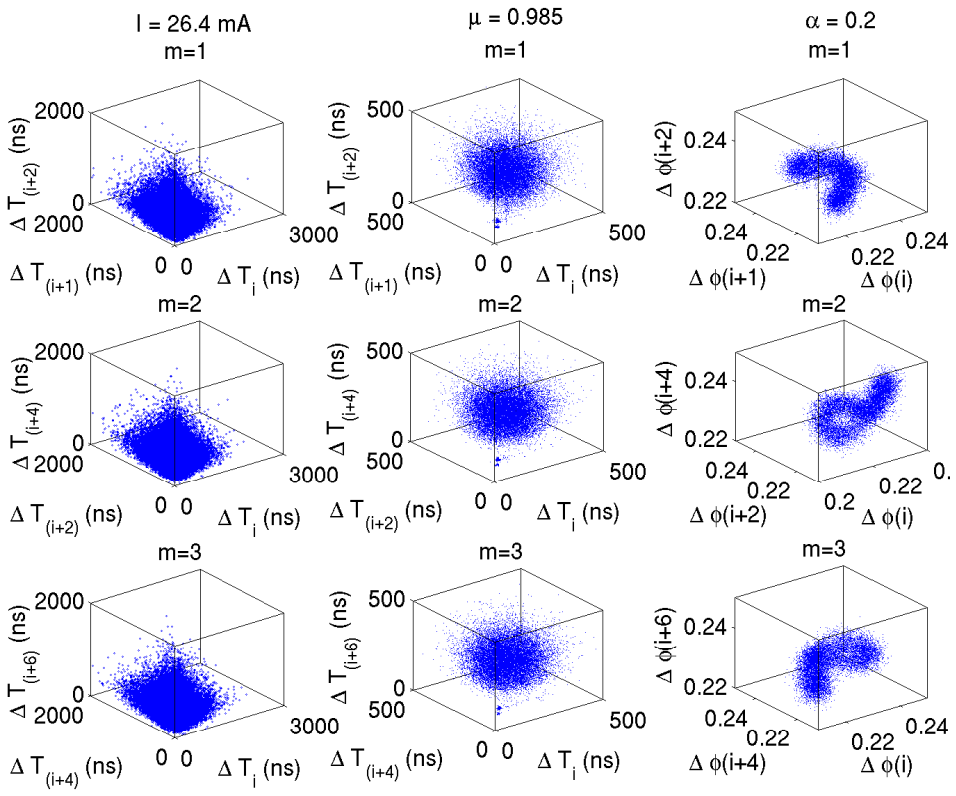

Figure 8: Three dimensional delay embedding of the inter-dropout interval time series for the experimental data (left column), for the numerical data (middle column), and for the minimal model (right column). For the minimal model, $\Delta\phi(i) = \phi(i) - \phi(i-1)$, following equation (3) from the main text.

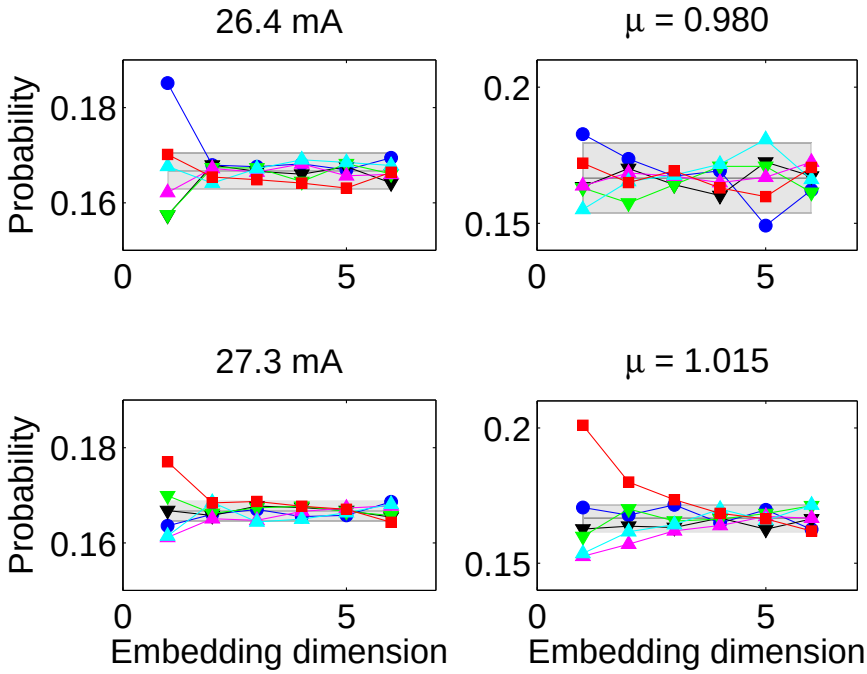

Figure 9: Probabilities of the words versus the delay (see text for details). Experimental data (left column), and numerical data (right column).

in this data set.

Also additional measurements were done including external forcing via direct modulation of the laser pump current. A 1550 nm semiconductor laser (Mitsubishi ML925B45F) was used, with feedback provided by an optical fiber. The feedback conditions were significantly different from those of the experiment reported in the main text. In this new experiment the feedback time delay was longer (25 ns), and the feedback stronger (threshold reduction being 11%). The dc value of the pump current was 12.50mA ($1.12I_{th}$) and temperature was 17 C. Figure 10d displays the probabilities vs. de pump current modulation amplitude and we can observe that, in spite of the fact that the experimental conditions are very different, there is a good qualitative agreement with Fig. 4 in the main text. For strong enough modulation amplitude, the hierarchy and clusters are the same in both data sets.

References

[1] Martinez Avila, J. F., de S. Cavalcante, H. L. D., Rios Leite, J. R., Experimental deterministic coherence resonance, *Phys. Rev. Lett.* **93**, 144101 (2004).

[2] Hong, Y. Shore, K. A., Statistical measures of the power dropout ratio in semiconductor lasers subject to optical feedback, *Opt. Lett.* **30**, 3332 (2005).

[3] Yacomotti, A. M., Eguia, M. C., Aliaga, J., Martinez, O. E. Mindlin G. B., Interspike time distribution in noise driven excitable systems, *Phys. Rev. Lett.* **83**, 292 (1999).

[4] Sukow D. W. and Gauthier D. J., Entraining power-dropout events in an external-cavity semiconductor laser using weak modulation of the injection current, *IEEE J. Quantum Electron.* **36** 175 (2000).

[5] Heil, T., Fischer, I., ElsäSSer, W., Dynamics of semiconductor lasers subject to delayed optical feedback: the short cavity regime, *Phys. Rev. Lett.* **87**, 243901 (2001).

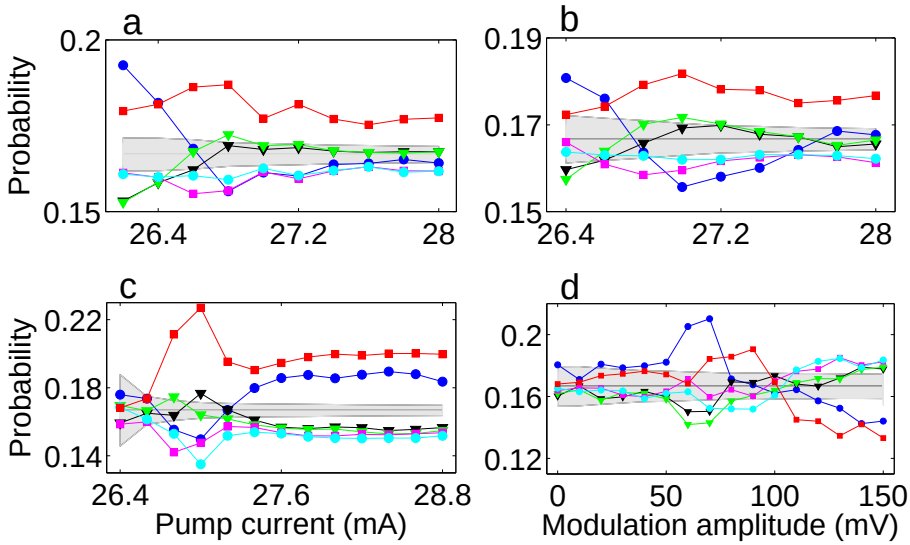

Figure 10: Words probabilities computed from data recorded using different experimental conditions. Panels (a) and (b) present the analysis of the data of ref. [7], recorded for two laser temperatures, **a** 18 C and **b** 20 C. The threshold reduction was 7% and the time delay 3 ns. the laser used was different from that refered to in the main text. The data analyzed in panel **c** was recorded using the same laser as in the main text, but with a different feedback level (threshold reduction of 4%). Time delay was 4.7 ns. The data analyzed in panel **d** correspond to a periodically modulated laser, emitting at telecom wavelength (1550 nm) and with optical feedback provided via an optical fiber that results in a threshold reduction of 11%. The feedback time delay was 25 ns and the laser was pumped at a dc current of 12.50 mA (equal to $1.12 I_{th}$).

[6] Takeda, A., Shogenji, R., Ohtsubo, J., Dynamics and pulse-package oscillations in broad-area semiconductor lasers with short optical feedback, *Appl. Phys. Lett.* **101**, 231105 (2012).

[7] Aragoneses, A., Rubido, N., Tiana-Alsina, J., Torrent, M. C., Masoller, C. Distinguishing signatures of determinism and stochasticity in spiking complex systems. *Sci. Rep.* **3**, 1778 (2013).

[8] Tim Sauer, Reconstruction of the dynamical systems from interspike intervals. *Phys. Rev. Lett.* **72**, 3811-3814 (1994).